

# A mobile robot with autonomous climbing and descending of stairs

## Pinhas Ben-Tzvi\*, Shingo Ito and Andrew A. Goldenberg

*Department of Mechanical and Industrial Engineering, University of Toronto, Canada*

(Received in Final Form: February 13, 2008. First published online: April 3, 2008)

### SUMMARY

Mobile robots are used to operate in urban environments, for surveillance, reconnaissance, and inspection, as well as for military operations and in hazardous environments. Some are intended for exploration of only natural terrains, but others also for artificial environments, including stairways. This paper presents a mobile robot design that achieves autonomous climbing and descending of stairs. The robot uses sensors and embedded intelligence to achieve the task. The robot is a reconfigurable tracked mobile robot that has the ability to traverse obstacles by changing its track configuration. Algorithms have been further developed for conditions under which the mobile robot would halt its motion during the climbing process when at risk of flipping over. Technical problems related to the implementation of some of the robot functional attributes are presented, and proposed solutions are validated and experimentally tested. The experiments illustrate the effectiveness of the proposed approach to autonomous climbing and descending of stairs.

**KEYWORDS:** Mobile Robots; Autonomous Systems; Control of Robotic Systems; Teleoperation; Design of Mechatronic Systems.

### 1. Introduction

Mobile robots have been developed for surveillance, reconnaissance, and inspection. Some are intended to explore not only natural terrains, but also artificial environments, including stairs and ramps. Traversing such urban obstacles has been a great challenge and inevitable difficulty to the improvement of mobility and expansion of operational range of mobile robots. In this paper, we present the development of autonomous climbing and descending of stairs with a Linkage Mechanism Actuator (LMA) tracked mobile robot developed with Engineering Services Inc. (ESI).<sup>1</sup>

Prior to the implementation of autonomous climbing, the LMA had two modes of operation: manual and preprogrammed. In the manual mode (remote control), the operator drives the LMA directly with the use of the remote controller. In the preprogrammed mode, a trajectory can be selected, parameters entered, and the LMA will follow the path automatically. During earlier operations and demonstrations of climbing and descending of stairs, only the manual mode was utilized. The operator navigates the LMA using the remote controller (joystick and buttons). The disadvantage of this mode is that the operator has to rely on his/her own judgment to set the robot in the right

configuration in order to be able to successfully climb and descend stairs without overturning. In addition, effecting this operation from a remote location, based only on the view of video images, provides a serious challenge to the operator. First, the operation in manual mode is intuitive, and it would be almost impossible to ascertain stability on climbing and descent. Second, climbing and descending stairs in the manual mode requires operator's knowledge, experience, skills and training. This is not preferred since the operators may have to be replaced from time to time. It is therefore advantageous to provide a robot with autonomous climbing and descending, thereby enabling precise, faster, and safer operation while reducing the operator's load and possible damage to the equipment in cases the robot might roll off the stairs.

To solve the issues raised, autonomous climbing and descending of stairs is proposed and successfully implemented.

### 2. Mechanical and Control Architecture of LMA

#### 2.1. Mechanical structure of LMA

Several mechanisms of robots to ascend stairs are currently available. Traversing stairs by connecting small identical robots is one approach.<sup>2,3</sup> Another unique strategy is a single miniature robot that jumps to traverse each step.<sup>4</sup> More commonly, robots with legs or leg and wheel combinations are used.<sup>5,6</sup> Tracked robots with special linkages are also widely used. Some robots such as the ROBHAZ-DT3 have uncontrollable linkages.<sup>7</sup> On the other hand, other robots such as PackBot,<sup>8,9</sup> Urban,<sup>10</sup> and Andros Mark VI<sup>11</sup> have an actuated linkage for additional tracks. The LMA also has an actuated linkage, but this is for reconfigurable tracks, not additional ones. This design approach provides the entire robotic platform with the ability to adjust its entire track configuration and therefore enhance traction when traversing different types of terrains such as stairs, steps, slopes, etc. It also provides the robot with the ability to vary its Center of Gravity (COG) location and thereby ensuring stability (as discussed in Subsection 3.1) throughout the different stages of climbing and descending of stairs.

Several views of the LMA are shown in Fig. 1. For the purpose of explanations, the side opposite to where the gray pole antenna is located is defined as the "front" (Fig. 1(b)), although the LMA is symmetrical in terms of its functions. The mobile robot has two fixed wheels at the front and rear of the chassis. Two arms are installed on both flanks of the frame, and two wheels are attached at their tip via a spring-loaded prismatic joint to retain tension in each track. The arms are rotated together in parallel to each

\* Corresponding author. Email: pinhas.bentzvi@utoronto.ca

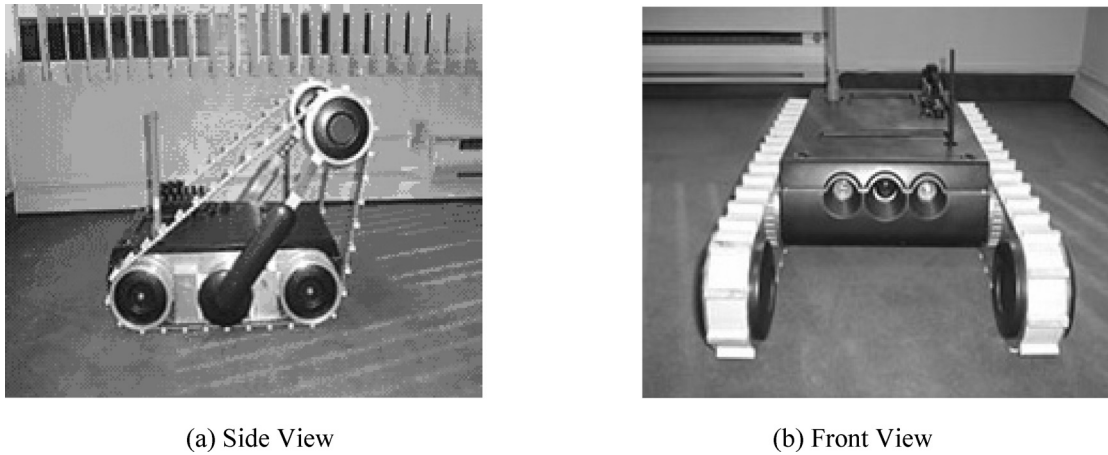


Fig. 1. Side and front views of the LMA.

other by one motor. The set of the two arms, including the attached joints and wheels mounted on them, is called the “flipper.” Two fixed wheels and one movable wheel are connected by a track on the left and right side of the frame, respectively. By rotating the flipper, the track configuration changes, which facilitates getting over obstacles, climbing and descending stairs and slopes. Each track is rotated by a motor independently, so that the LMA can not only go forward and backward, but also turn left, right, and around.

**2.1.1. Relationship of flipper angle and length.** The location of the robot’s Center of Gravity (COG) changes as the flipper rotates. Since the COG location is utilized in the derivation of the stability judgment equations for autonomous climbing and descent in Section 3, it is required to know the relationship between the flipper angle and its length. The tracks are flexible enough to allow the flipper rotation, but their length never changes. Therefore, the flipper tip follows an ellipsoid trajectory. The parameters used to find the relationship between the flipper angle and its corresponding length are defined in Fig. 2. The flipper angle is denoted by  $\varphi$  and the flipper length is denoted by  $l(\varphi)$ . In a  $x$ - $y$  coordinate frame, whose origin is located at the joint of the flipper as shown in Fig. 2, the ellipsoid trajectory of the centers of the flipper wheels can be expressed by the following equation:

$$\frac{x^2}{a^2} + \frac{y^2}{b^2} = 1 \quad (1)$$

In order to relate the flipper angle to its length with the above equation, a polar coordinate frame is located at the same point as that of the  $x$ - $y$  coordinate frame, and is defined as  $x = l(\varphi) \cos \varphi$ ,  $y = l(\varphi) \sin \varphi$ . With these relations substituted into Eq. (1) and solved for  $l(\varphi)$ , we get:

$$l(\varphi) = \sqrt{\frac{a^2 b^2}{b^2 \cos^2 \varphi + a^2 \sin^2 \varphi}} \quad (2)$$

Relevant specifications of the LMA are provided in Table I.

## 2.2. Computer architecture of the LMA

Figure 3 shows the on-board hardware architecture and signal flows of the LMA including the Operating Control

Table I. General specification of the LMA.

Name	Parameter	Dimension
Wheelbase	L	400 mm
Longest Flipper Length	a	466 mm
Shortest Flipper Length	b	421 mm
Wheel Radius	r	74 mm
Weight	w	34.0 kg

Unit (OCU). An operator inputs commands with the remote controller (joystick and buttons), and the commands are encoded into a 16-byte data set called “frame”, which are transmitted to the robot via the antennas and received and decoded by the slave controller.

If the decoded commands by the slave controller include a request for a sensor, the slave controller sends a corresponding request to the sensor processor, which continuously holds up-to-date data from all the sensors. Then the sensor processor returns the particular sensor’s data to the slave controller and encodes the received data to transmit to the remote master controller.

In cases were the transmitted frame to the LMA includes commands to operate the motors, the slave controller sends corresponding signals to the proper drivers to drive the motors. Of the three motors situated in the robot chassis,

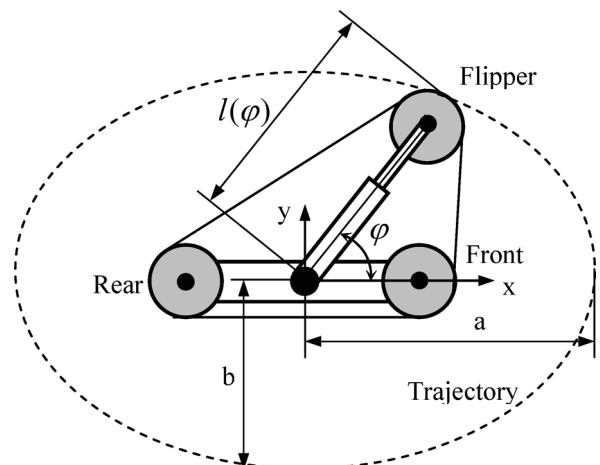


Fig. 2. Parameters for flipper length calculation.

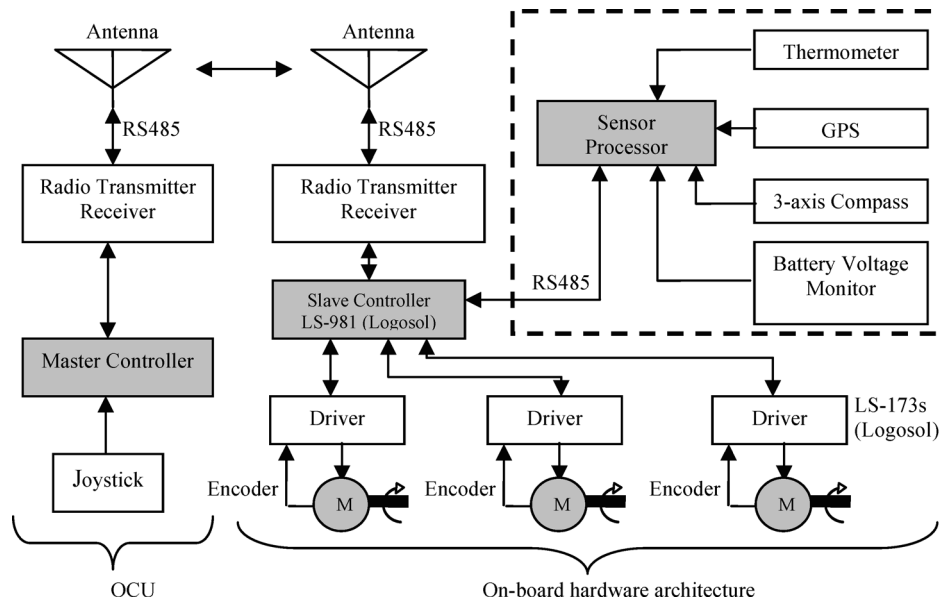


Fig. 3. Hardware architecture of the LMA.

two motors are propelling the left and right tracks and the third one is propelling the flipper. Encoders connected to the motors are utilized to establish closed-loop position, speed or acceleration control of the motors.

Logosol’s LS-991 and LS-981<sup>12</sup> were used as the master and slave controllers, respectively. Both are equipped with Rabbit 2000 CPU and are programmable with Dynamic C. Three LS-173s drivers are used to control the motors and are controlled via the slave controller.

*Sensors*

Rabbit 3000 CPU mounted on RMC3400 Rabbit Core is used as the sensor processor. The processor is 29.4 MHz and programmable with the use of Dynamic C. The capacity of the memories mounted on the core package is 512 KB for both SRAM and flash memory.

The LMA is equipped with a thermometer, GPS, three-axis compass, and battery–voltage monitor. The three-axis compass manufactured by Honeywell is tilt-compensated. It provides pitch, roll, and yaw (heading direction) angle with a sampling frequency of 8 Hz. The range of the heading direction is 360° and that of roll and pitch angles is ±60°. The package is composed of single and two-axis magnetic sensors, as well as a two-axis accelerometer.

*2.3. Procedure for climbing and descending stairs*

The schematic in Fig. 4 shows the stair profile used and some related parameters. The height of each step or riser length ranges from 12–18 cm and the width of a step ranges from 8–25 cm. The imaginary line connecting the stair edges is referred to as the “nose line.” The slope of a nose line indicates how steep the stairs are, and its range is from 25–45°. Stairs with step height and width of 18 cm and nose line slope of 45° were used to test the LMA.

The motions required to climb stairs are broken down into three stages—the “riding on nose line,” “going on nose line,” and “landing” stage. Figure 5 shows each procedure to climb stairs.<sup>2</sup>

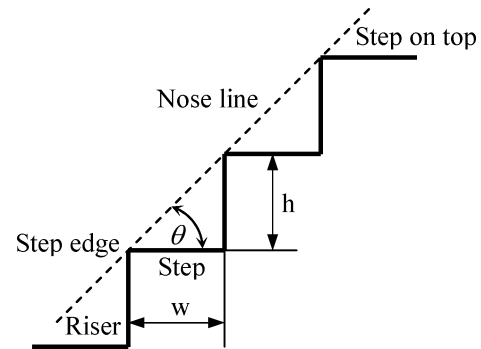


Fig. 4. Stair profile and parameters.

In the riding on nose line stage, the LMA moves forward until its front wheels are above the first step edge as shown in Fig. 5(a), (b), and (c). During the motion, the flipper is set at a certain angle ( $\varphi$  is approximately 45°) at the front, such that some of the treads on the tracks engage onto the first step edge. The flipper is then rotated backwards until its tip touches the ground to avoid flipping over (Fig. 5(d)), and then the LMA moves forward (Fig. 5(e)). We observed during various experiments that the COG position change during the flipper’s motion between configurations 5(c) and 5(d) did not pose any flip over instability issues. At a proper time, the LMA is stopped and the flipper is extended to the rear to ride on the nose line as shown in Fig. 5(f).

After the completion of the riding on nose line stage, the LMA moves forward on the nose line (going on nose line stage). The LMA maintains this stage until the front wheels are suspended above the step at the top. During this stage, the operator would be required to adjust the heading direction of the LMA, for example, in cases of curved or spiral stairs. According to observations during various autonomous stair climbing and descending experiments, as long as the LMA started at the center of the stairs, it finished sufficiently close to the staircase centerline. In cases where the trajectory disturbances due to the dynamic motion profile causes the

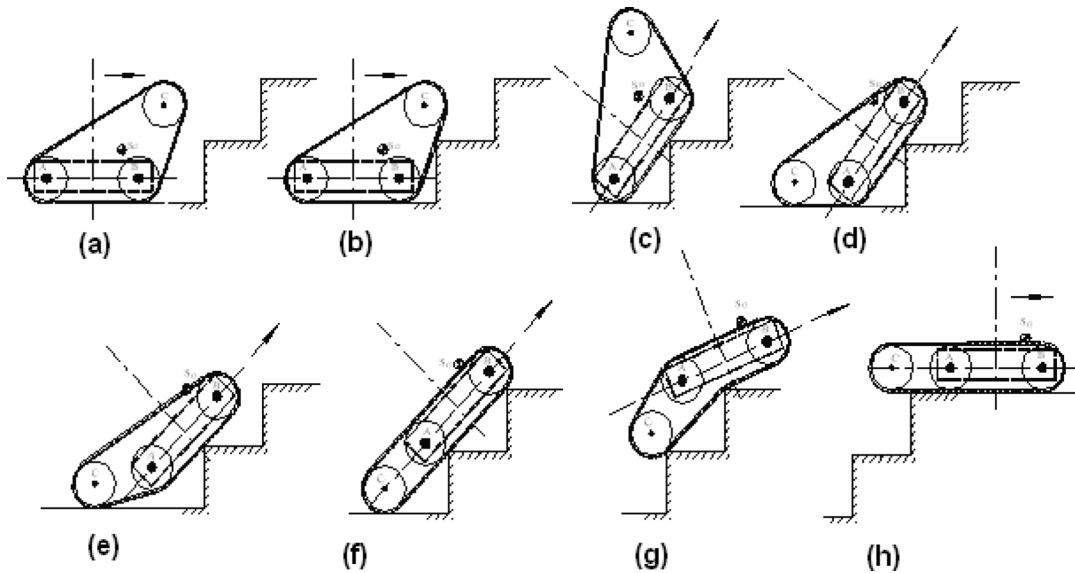


Fig. 5. Climbing and descending procedures for stairs: Climbing follows the order of (a), (b), (c), (d), (e), (f), (g) and (h); Descending follows the order of (h), (g), (f), (e), (d), (c), (b) and (a).

robot to move toward the boundaries of the staircase, in order to avoid collisions with the walls or the stair railing, it may be necessary to measure the robot's heading angle and provide appropriate correction. This may be accomplished by designing a heading feedback controller so as to minimize the heading error and guarantee that the robot will travel straight up the stairs. The heading controller may receive as input the heading reference direction and the real-time measurements of the yaw (heading) angle from the three-axis compass as a feedback. The output of the heading controller would be the commanded rotational velocities of the robot's tracks.

The purpose of the landing stage is to prevent the front wheels to hit the step at the top. In order to do so, the flipper is slightly rotated downward as shown in Fig. 5(g). Subsequently, the LMA moves forward until its rear wheels are completely placed on the step at the top, and its flipper extends to the rear (Fig. 5(h)). In cases where "hard landing" is acceptable, it may not be necessary for operators to follow the landing procedure.

The procedure for descending stairs is accomplished by a backward sequence of the steps required to climb the stairs (Fig. 5). In this case, the robot may descend from its tail, or

rear with no need to rotate it in order to descend with its front forward after climbing the stairs.

### 3. Stability Analysis for Autonomous Climbing and Descending of Stairs

During autonomous climbing and descending of stairs, there is a considerable probability that the LMA would fall off or flip over. To address this scenario and relate it to the configuration and inclination of the robot on stairs, "stability judgment" equations were formulated for different robot configurations. These equations are providing the inclination thresholds that may result in robot instability. Using these thresholds, the LMA can be successfully stopped before it is in danger of rolling over or falling off. The required equations and algorithms are derived and introduced in this section.

#### 3.1. Stability judgment equations

3.1.1. Stability judgment equation of LMA with flipper suspended above the platform. The configuration to be considered is shown in Fig. 6(a). The front wheels are on the first step edge and the flipper is raised above the platform.

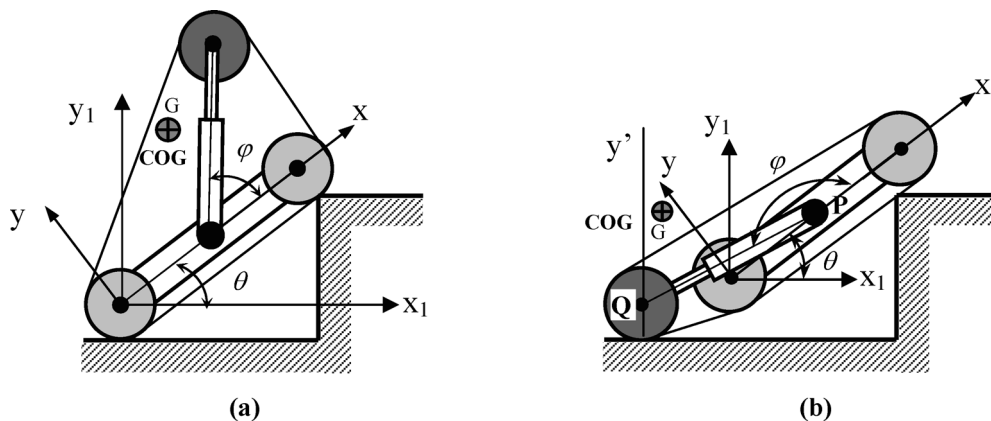


Fig. 6. (a) LMA with front wheels on step edge; (b) LMA with flipper wheels at the rear.

A Cartesian coordinate frame is aligned with the origin located at the center of the rear wheels' axis and its  $x$  axis is parallel with the robot's longitudinal axis. With respect to this coordinate frame, the location of center of gravity of the LMA (shown as a dark circle in Fig. 6(a)) is expressed as  $G_x$  and  $G_y$  with respect to  $x$  and  $y$  axis, respectively. The origin of the inertial Cartesian coordinate frame  $(x_1, y_1)$  is located at the center of the rear wheels and their axes are oriented as shown in Fig. 6(a).

The coordinate of the COG on  $x_1$  axis is given by:

$$G_{x1} = G_x \cos \theta - G_y \sin \theta \quad (3)$$

where  $\theta$  is the robot's inclination, which is measured by the three-axis compass. To avoid flipping over from the first step on the stairs, the COG must be maintained with a positive  $x_1$  coordinate  $G_{x1} > 0$ . Substituting this condition into Eq. (3) and solving yields the following stability judgment equation:

$$G_x > G_y \tan \theta \quad (4)$$

**3.1.2. Stability judgment equation of LMA with flipper at rear.** The configuration considered in this case is shown in Fig. 6(b). In this configuration, the LMA chassis has inclination  $\theta$ , flipper angle is  $\varphi$  (between  $90^\circ$ – $270^\circ$ ), and the tip of the flipper supports the LMA on the ground. Two coordinate frames,  $x - y$  and  $x_1 - y_1$ , are aligned in the same manner as in Fig. 6(a). The location of the COG in  $x_1 - y_1$  coordinate frame (i.e.,  $G_{x1}$  and  $G_{y1}$ ) is expressed below, relating its coordinates to the  $x - y$  coordinate frame:

$$\begin{aligned} G_{x1} &= G_x \cos \theta - G_y \sin \theta \\ G_{y1} &= G_x \sin \theta + G_y \cos \theta \end{aligned} \quad (5)$$

The coordinate of  $P$ , the point of rotation of the flipper, is expressed in  $x_1 - y_1$  coordinate frame as follows:

$$\begin{aligned} P_{x1} &= \frac{L \cos \theta}{2} \\ P_{y1} &= \frac{L \sin \theta}{2} \end{aligned} \quad (6)$$

where  $L$  is the wheelbase. The position of the point  $Q$ , which is the center of the flipper wheel, is given below:

$$\begin{aligned} Q_{x1} &= P_{x1} + l(\varphi) \cos(\varphi + \theta) = \frac{L}{2} \cos \theta + l(\varphi) \cos(\varphi + \theta) \\ Q_{y1} &= P_{y1} + l(\varphi) \sin(\varphi + \theta) = \frac{L}{2} \sin \theta + l(\varphi) \sin(\varphi + \theta) \end{aligned} \quad (7)$$

where  $\varphi$  and  $l(\varphi)$  are the flipper angle and flipper length, respectively.

To avoid flipping over of the robot, the COG must be maintained at the right side of the line  $y'$  as indicated in Fig. 6(b). In order to accomplish this, the condition  $G_{x1} > Q_{x1}$  must be satisfied.

or

$$G_x \cos \theta - G_y \sin \theta > \frac{L \cos \theta}{2} + l(\varphi) \cos(\varphi + \theta) \quad (8)$$

Solution of the above equation for  $G_x$  yields the following stability judgment equation:

$$G_x > G_y \tan \theta + \frac{L}{2} + l(\varphi) \frac{\cos(\theta + \varphi)}{\cos \theta} \quad (9)$$

**3.1.3. Stability judgment equation of LMA on nose line.** The required conditions for stability of mobile robots on the nose line have been generated.<sup>13-15</sup> These conditions are primarily as follows: (i) half the wheelbase of a mobile robot is larger than the distance of two adjacent step edges (Condition 1); (ii) mobile robot's COG is over the step edge which the robot engages rearward (Condition 2). The interaction between the tracks and the stairs, which is affected by the shape characteristics of the tracks, the contact forces, and the capacity of the generated wheel torques that drive the tracks ensured sufficient tractive forces for successful climbing. The sufficiency of the tractive force to balance the gravity was validated by the robot's ability to successfully climb and descend stairs throughout the entire range of the climbing and descending experiments.

The first condition guarantees that the LMA stays on the nose line, so that it always contacts at least two-step edges. In the application of the LMA, this condition can be illustrated with the aid of Fig. 7(a). The distance between the front

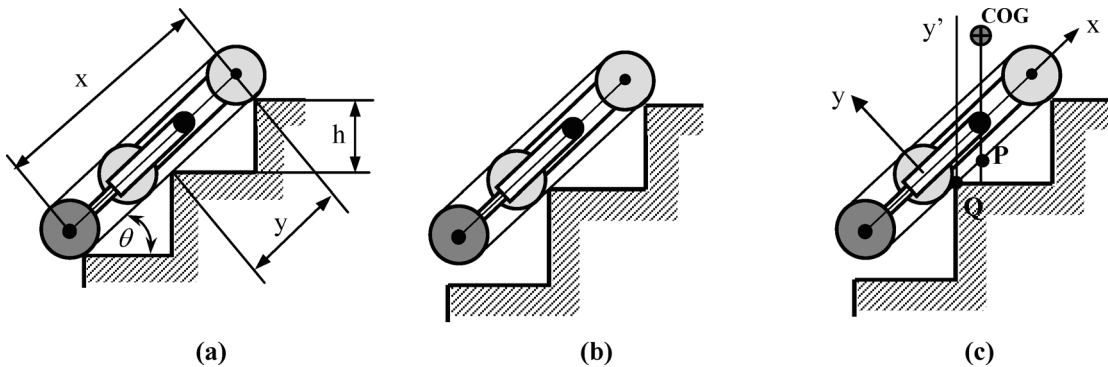


Fig. 7. (a) LMA on nose line; (b) Exception; (c) LMA COG location.

wheels and the flipper wheels, while the LMA is moving on a nose line, is denoted as  $x$ , and is given by:

$$x = \frac{L}{2} + l(180^\circ) - r \quad (10)$$

The slope of the nose line  $\theta$  coincides with the inclination of the LMA; therefore, it can be measured by the three-axis compass. Using this measurement and the step height  $h$ , the distance between two adjacent step edges  $y$  is given by:

$$y = \frac{h}{\sin \theta} \quad (11)$$

With Condition 1 mentioned above, the following equation must be satisfied for stable climbing or descent:

$$x \geq 2y \quad (12)$$

By substituting Eqs. (10) and (11) into Eq. (12), and solving for  $\theta$  we get:

$$\theta \geq \sin^{-1} \frac{2h}{L/2 + l(180^\circ) - r} \quad (13)$$

The derived equation is a moderate constraint. Even if it is slightly violated, the LMA can still climb or descend stairs. This can be explained visually. In Fig. 7(b), the distance between two adjacent step edges is greater than half the distance between the flipper wheels and the front wheels, such that Eq. (13) is violated. Nevertheless, the LMA can still climb by engaging some of the track treads onto the step edge in front of it. In other words, condition (13) has a margin. Beyond that margin, the LMA stops since it gets stuck in the spaces between the stairs.

Condition 2 above assures that the LMA does not flip over on the stairs when climbing or descending. As shown in Fig. 7(c), The COG of the LMA must stay on the right side of  $y'$  line before the flipper wheels disengage from the stair edge. The  $x$  coordinate of point  $Q$ , at which the track contacts the step edge, is expressed as follows:

$$Q_x \leq \frac{L}{2} - l(180^\circ) + \frac{h}{\sin \theta} \quad (14)$$

Similarly, the  $x$  coordinate of the point  $P$ , where the nose line crosses the vertical line from the COG, is given by the following equation:

$$P_x = G_x - (G_y + r) \tan \theta \quad (15)$$

To keep the stable position in the figure, the COG must be located on the right side of the  $y'$  axis. Therefore, the following equation must be satisfied:

$$P_x > Q_x \quad (16)$$

By substituting Eqs. (14) and (15) into Eq. (16) and solving for  $G_x$ , the following stability judgment equation is derived:

$$G_x > \frac{L}{2} - l(180^\circ) + \frac{h}{\sin \theta} + (G_y + r) \tan \theta \quad (17)$$

**3.1.4. Relation of robot inclination and flipper angle on ground.** In this section, an equation is derived in order to relate robot inclinations to the flipper angle, when the flipper supports the robot on the ground. The configuration to be considered as an illustration is shown in Fig. 8. In the figure, the LMA is inclined and its flipper sustains the body. A coordinate frame is aligned at the center of the rear wheels with the  $x$  axis parallel to the ground. The coordinates of the points  $S$  and  $Q$  (the centers of the front and flipper wheels, respectively) on the  $y$  axis are given by the following expressions:

$$S_y = -L \sin(-\theta)$$

$$Q_y = -\frac{L}{2} \sin(-\theta) - (l(\varphi) - r) \sin(\varphi + \theta - 180^\circ) \quad (18)$$

Since both the centers of the front and flipper wheels are situated on the same ground level, the following relationship is satisfied:

$$S_y = Q_y \quad (19)$$

Solving the above equations for the inclination angle  $\theta$  yields:

$$\theta = \tan^{-1} \frac{\sin \varphi}{\frac{L}{2(l(\varphi) - r)} - \cos \varphi} \quad (20)$$

Equation (20) was utilized to stop the LMA at the top of the stairs (Fig. 5(g)), at which time its configuration is similar to the one shown in Fig. 8.

An experiment was conducted in order to examine the accuracy of Eq. (20). The experiment involved the following steps: (i) set LMA on a horizontal ground with flipper at the rear (i.e.,  $\varphi = 180^\circ$ ); (ii) rotate the flipper  $5^\circ$  downwards; (iii) wait 3 seconds and measure the inclination; (iv) repeat steps (ii) and (iii) until the flipper angle becomes  $230^\circ$ . This experiment was done twice, and the averages of the measured inclinations for each flipper angle were calculated.

From the results shown in Fig. 9, we observe that the deviation between theoretical values and measured values of the inclination is increasing as the flipper angle increases. The flipper angle, with which Eq. (20) is utilized to stop the LMA during the landing stage in Fig. 17, is  $225^\circ$ . According to Fig. 9, the difference between the theoretical and measured data is only  $1.7^\circ$  when the flipper angle is  $225^\circ$ . Also, the measured inclinations are smaller than the theoretical inclination. Therefore, the LMA can be stopped with the condition of Eq. (20) after landing is completed, considering

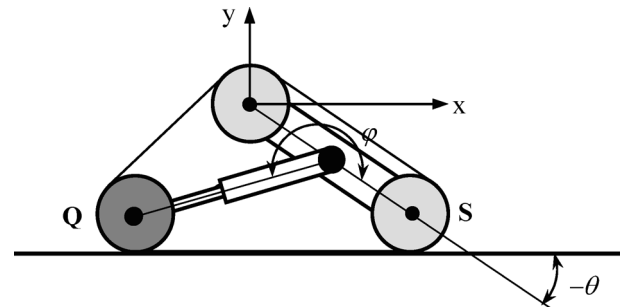


Fig. 8. LMA with flipper supporting its body.

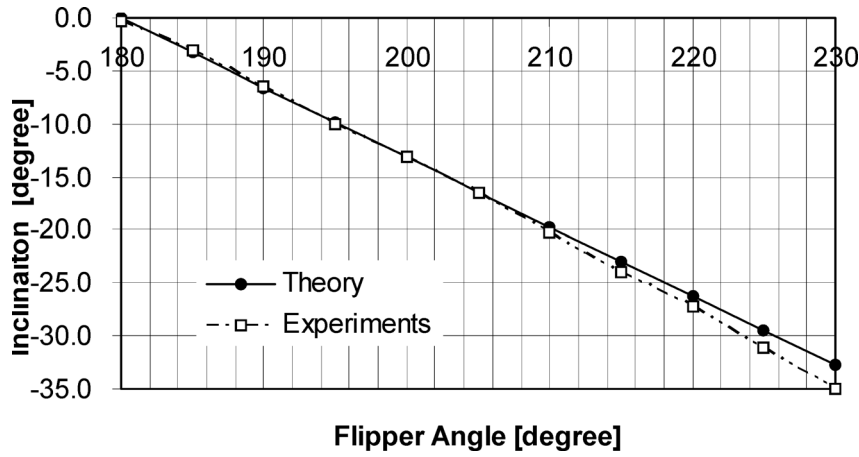


Fig. 9. Robot inclination vs. flipper angle—validation of Eq. (20).

also the settling time of the compass. In fact, successful stops were consistently observed during autonomous climbing.

The stability judgment equations derived in this subsection contain variables of the COG coordinates. Since the position of the robot's COG is a function of the flipper angle, the COG coordinates need to be obtained in real-time, but this may increase the computational load. To avoid this real-time task, the range in which the robot's COG varies was identified and used.

### 3.2. Range of COG coordinates

In order to find the COG range, the relationship between the robot's COG position and its flipper angle was derived. To do that, LMA is imaginarily decomposed into two parts: the flipper and the rest (platform). The mass of the flipper is denoted  $m_F$ , and the position of its COG  $G_F$  in the coordinate frame shown in Fig. 10(a). Similarly, the platform's mass is denoted  $m_P$  and its COG position  $G_P$  (Fig. 10(b)). Using these parameters, the COG of the LMA can be expressed by Eqs. (21) and (22). It is assumed that the weight of the track is included in that of the platform.

$$G_x(\varphi) = \frac{m_P G_{Px} + (L/2 + G_{Fx} \cos \varphi) m_F}{m_P + m_F} \quad (21)$$

$$G_y(\varphi) = \frac{m_P G_{Py} + m_F G_{Fy} \sin \varphi}{m_P + m_F} \quad (22)$$

Equation (21) implies that the  $x$  coordinate of the COG is maximum and minimum when the flipper angle  $\varphi$  is 0 and 180°, respectively. Similarly, the  $y$  coordinate of the COG indicates that the maximum and minimum occur when the flipper angle  $\varphi$  is 90° and 270°, respectively.

The COG of the LMA always stays in the range defined by the four values above. Therefore, with these constant values, a real-time computation of the COG position can be avoided and Eqs. (4), (9), (13) and (17) are replaced by the following equations:

$$G_{x \min} > G_{y \max} \tan \theta \quad (23)$$

$$G_{x \min} > G_{y \max} \tan \theta + \frac{L}{2} + l(\varphi) \frac{\cos(\theta + \varphi)}{\cos \theta} \quad (24)$$

$$G_{x \min} > \frac{L}{2} - l(180^\circ) + \frac{h}{\sin \theta} + (G_{y \max} + r) \tan \theta \quad (25)$$

The procedure to measure the COG of a motorbike was utilized<sup>16</sup> in order to find the COG range of the LMA as a function of the flipper angle. The minimum ordinate of the COG was not measured since it is not required in the derived stability judgment equations. The calculated range of the COG is summarized in Table II.

### 3.3. Algorithms for stability judgments

During autonomous climbing and descending of stairs, some computer tasks are simultaneously running, these include: sending requests to the compass, receiving frames from the sensor and the remote controller and judging stability, as well as executing autonomous climbing or descending procedures. In this section, the stability judgment equations derived in Subsections 3.1 and 3.2 are used in algorithms developed in order to prevent the LMA from falling or flipping over during the different stages of climbing and descending of stairs.

The derived stability judgment equations corresponding to the robot's configuration are continuously evaluated based on up-to-date robot's inclination measurements, while the robot is moving. The robot responds differently once any of the derived equations (i.e., Eqs. (13), (23), (24), and (25)) is violated. For instance, if Eqs. (23) or (24) (represent the stability judgment equations of the LMA with the flipper suspended above the platform and flipper located at the rear, respectively) are not satisfied, the LMA stops right away, and autonomous climbing or descending is terminated. This algorithm is named stability judgment thread 1 (abbreviated as S.J.T.1 in subsequent flowcharts), and its corresponding flowchart is shown in Fig. 11(a).

In the case when Eqs. (13) or (25) (represent the stability judgment equations of the LMA when moving

Table II. Calculated parameters of COG range.

Parameter	$G_{x, \max}$	$G_{y, \max}$	$G_{x, \min}$
Value	25.9 cm	1.5 cm	19.3 cm
Scale values used at Flipper Angle of	0	90°	180°

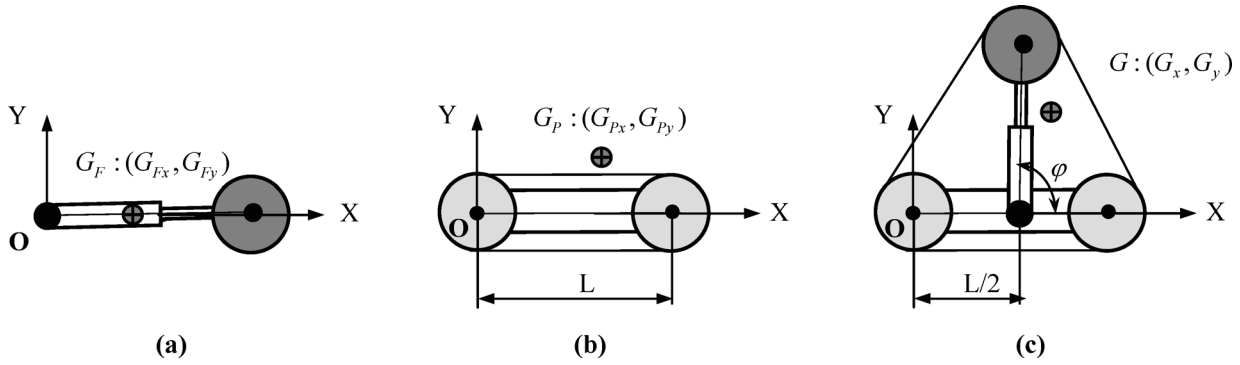


Fig. 10. LMA decomposition and COGs.

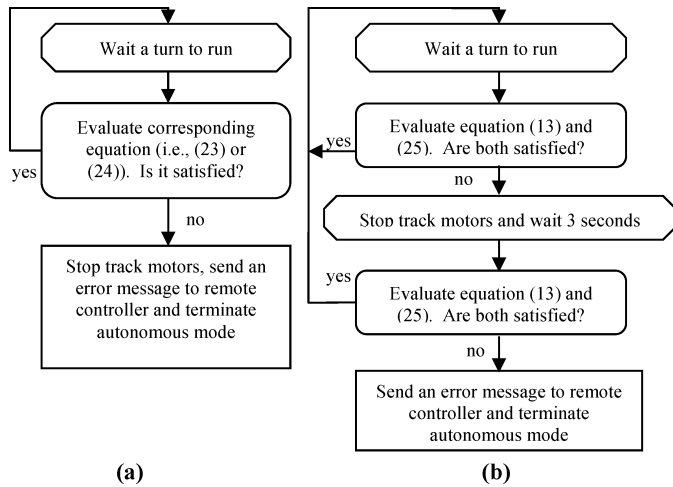


Fig. 11. (a) Stability judgment thread 1; (b) Stability judgment thread 2.

on the nose line) are violated, the LMA stops right away and waits 3 s followed by another evaluation of both equations. If either equation is still not satisfied, autonomous climbing or descending is terminated; otherwise, the LMA continues its motion. This algorithm is called stability judgment thread 2 (abbreviated as S.J.T.2 in subsequent flowcharts) and summarized in the flowchart shown in Fig. 11(b).

A margin has been incorporated in this algorithm in order to overcome noise effects associated with robot inclination measurements, while the LMA is climbing or descending stairs on a nose line. Therefore, the validation on the effectiveness of this algorithm and the stability judgment equations is presented in Section 5, following the analysis of

the noise in the robot inclination signal measurements and discussion on the techniques that were employed in order to filter it.

#### 4. Algorithms for Autonomous Climbing and Descending of Stairs

##### 4.1. Algorithms for autonomous climbing of stairs

During autonomous climbing, the LMA depends on measurements from its inclinometer (the three-axis compass) and the encoders attached to the three motors. The algorithm to autonomous climbing is divided into four stages: measurement of step height, riding on the nose line, going on the nose line and landing. The stability judgment equations derived in Section 3 are incorporated in the algorithms as well.

##### 4.1.1. Climbing task stage 1: measurement of step height.

In the first stage of autonomous climbing, the step height of the stairs is measured. In the initial position, the flipper is positioned at the rear, and the LMA is located in front of the first riser by the operator, such that the two tracks touch the riser. The autonomous process starts when the LMA moves backwards 10 cm and the flipper (Fig. 12(a)) rotates to the front until its angle is set to 60°.

The flipper is then rotated further downwards with open-loop control in a manner such that its torque is small enough to stop the flipper’s rotation when it touches the first step edge (Fig. 12(b)). The motor is turned off when eight seconds are elapsed from the time the open-loop control is initiated. If during that time the flipper is extended to the front (i.e.,  $\varphi = 0^\circ$ ), the flipper motor is turned off, an emergency error is sent to the remote controller, and autonomous climbing terminates since the LMA considers that there are no stairs.

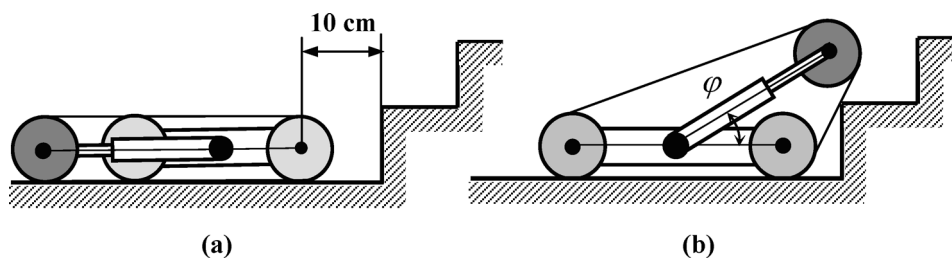


Fig. 12. Step height measurement.

If an emergency error is not invoked, the step height is calculated from the flipper angle, and the value is labeled as  $h$ . Consequently, the calculated stair height is transmitted to the remote controller, and the flipper angle is reset to  $45^\circ$ . The equation used for step height measurement was derived with the use of the least square method and experiments, as discussed in Subsection 5.1.

This algorithm is summarized and shown in a flowchart in Fig. 13. While the motors are rotating, other tasks can run simultaneously in a multitasking procedure. The motor rotations are represented by octagon shapes in the flowcharts.

4.1.2. Climbing task stage 2: riding on the nose line.

Following the stair height measurement, LMA rides on the nose line by first positioning the robot as shown in Fig. 14(a). During the motion, the stability judgment thread 1 (shown in Fig. 11(a)) is running with Eq. (23). The total distance

the LMA needs to traverse was verified empirically, and was found to be the measured stair height plus 15 cm.

To prevent flipping over, the flipper is rotated backwards by setting its angle to  $160^\circ$ . After this rotation is completed, the inclination of the robot is recorded for autonomous descending, and the value is labeled as  $\theta_1$ .

Along with the stability judgment shown in Fig. 11(a) and Eq. (24), the LMA restarts in order to complete the riding on the nose line stage completely, and then stops on the nose line (Fig. 14(b)). There are three conditions to stop the LMA as indicated in the flowchart in Fig. 15.

After the LMA rides on the nose line (Fig. 14(b)), its flipper is rotated backwards until its angle is set to  $180^\circ$  to guarantee a more stable configuration on the nose line. The flowchart for this algorithm is shown in Fig. 15. The octagon shapes for multitasks in the flowchart are used to indicate the interruption of the flipper rotations.

4.1.3. Climbing task stage 3: going on nose line. In this stage, the LMA moves forward on the nose line and measures the slope of the nose line. Since the signal from the three-axis compass is noisy, an average of the measured data is used.

The first motion of this stage is to move forward 50 cm, to assure that the flipper tip is detached from the ground. Then, the LMA moves forward again while continuously measuring the inclinations. The forward motion velocity is set to 3.2 cm/s and regulated by the closed-loop control of the drivers. During the motion, the stability judgment thread 2 shown in Fig. 11(b) is running.

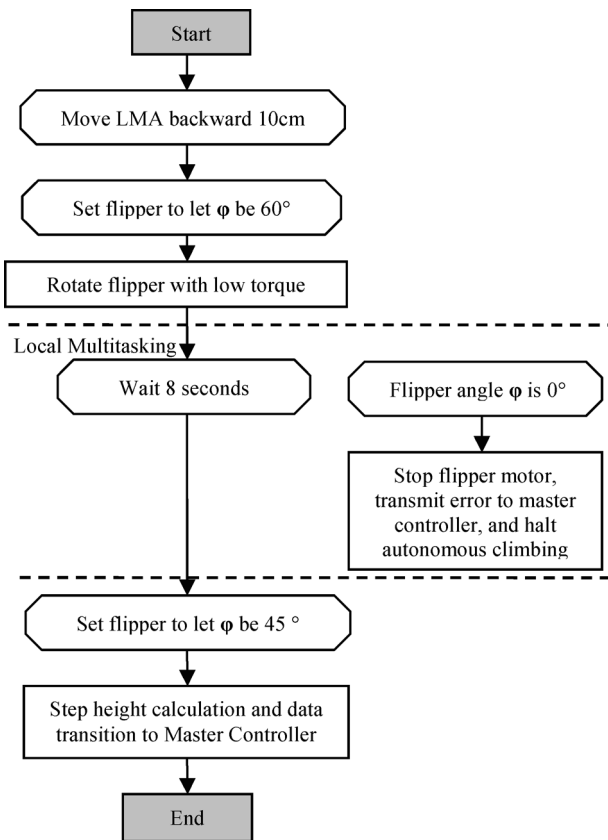


Fig. 13. Flowchart of step height measurement stage.

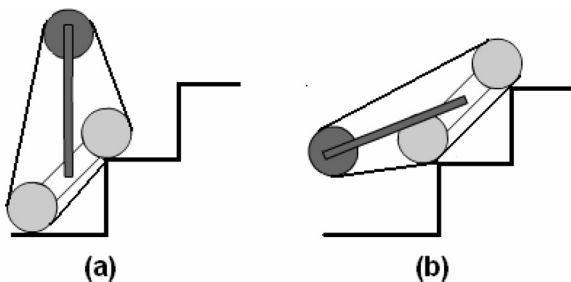


Fig. 14. Riding on nose line of autonomous climbing.

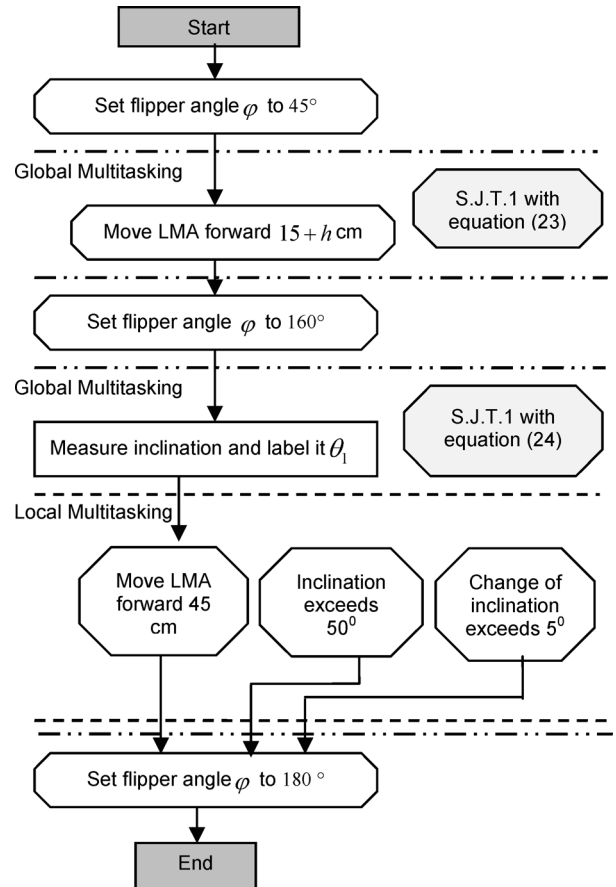


Fig. 15. Flowchart of riding on nose line climbing stage.

Since the LMA is equipped with only the three-axis compass and encoders for the motors, it cannot detect the last step of the stairs. Therefore, the LMA is stopped by the operator when its front wheels are above the last step edge, at which time automatic landing stage is activated. Otherwise, the LMA tracks will abruptly drop on the top step. In that case, the LMA would automatically stop and autonomous climbing of stairs is completed. The flowchart for going on nose line stage is shown in Fig. 16.

4.1.4. *Climbing task stage 4: landing.* After the operator stops the LMA as shown in Fig. 17(a), the operator initiates the landing stage. First, the flipper rotates to set its angle to  $225^\circ$  (Fig. 17(b)) and the LMA moves forward until its inclination becomes  $-28^\circ$  or less, under which the LMA is completely on the last step as shown in Fig. 17(c). This inclination value of  $-28^\circ$  was found by substituting  $\varphi = 225^\circ$  into Eq. (20) and adding  $1.5^\circ$  as a margin. The rest of the steps are summarized in Fig. 18.

4.2. Algorithms for autonomous descending of stairs

Autonomous descending of stairs relies on the information collected during autonomous climbing of stairs (i.e., step height  $h$ , the inclination  $\theta_1$  and the slope of the nose line). The algorithm for autonomous descending of stairs can also be separated into three stages—namely, riding on the nose line, going on nose line and landing.

4.2.1. *Descending task stage 1: riding on the nose line.* The LMA does not need to rotate after autonomous climbing of stairs since it autonomously descends the stairs from its rear with the flipper positioned at the rear.

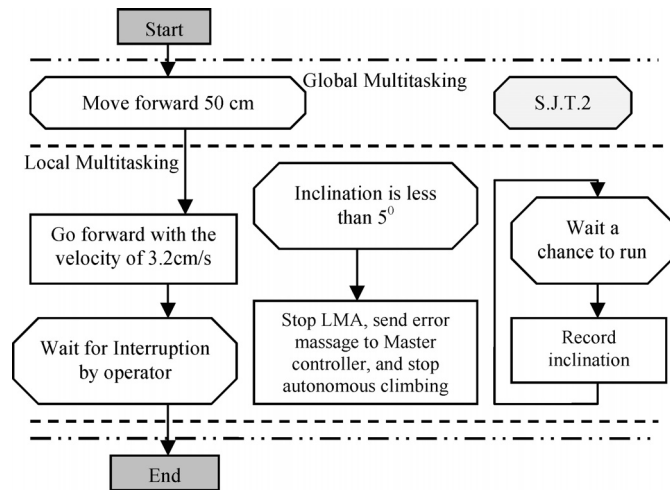


Fig. 16. Flowchart of going on nose line climbing stage.

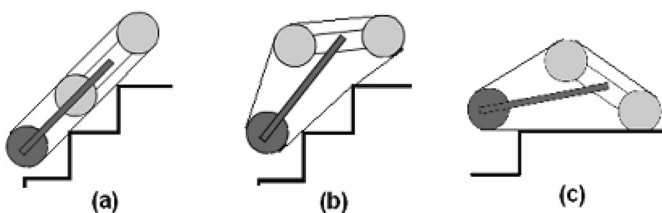


Fig. 17. Landing stage of autonomous climbing.

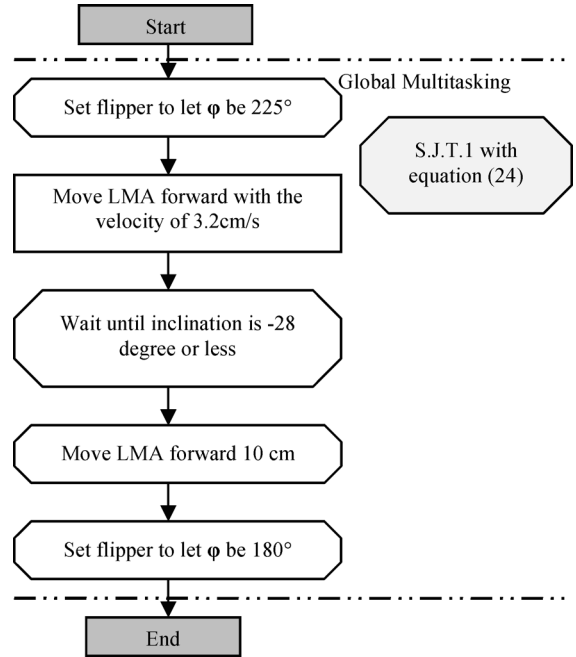


Fig. 18. Flowchart of stair climbing landing stage.

First the flipper is rotated until its angle is set to  $215^\circ$  (Fig. 19(a)). With the stability judgment thread 1 (with Eq. (24)), the LMA moves backwards with a speed of 3.2 cm/sec to approach the stairs and descend its first step (Fig. 19(b)). When its inclination becomes greater than  $-10^\circ$ , the LMA interprets that as having descended the first step and it stops. This inclination value was found empirically, and is expected to be ideal for any stairs under the assumptions made in Section 3. Then the flipper is extended to the rear as shown in Fig. 19(c).

If during the backward motion of the LMA the three-axis compass does not show a value less than  $-10^\circ$ , the movement stops automatically and the robot transmits an error message to the OCU that no stairs have been detected. The flowchart for this stage is shown in Fig. 20.

4.2.2. *Descending task stage 2: going on nose line.* After the LMA completes riding on the nose line, it moves backwards until its inclination is less than the nose line's slope (the average of the recorded inclinations during climbing) minus  $7^\circ$ . The  $7^\circ$  is taken as a margin derived from several trials. After the LMA stops, it waits 3 s and judges if the up-to-date inclination is less than the threshold. If so, the next stage is initiated; otherwise the LMA starts to move backwards again. The decrease in the robot's inclination is caused when the

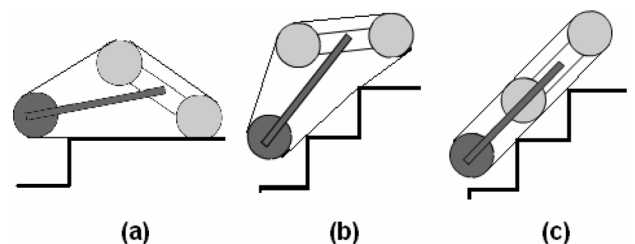


Fig. 19. Riding on the nose line of Autonomous descending.

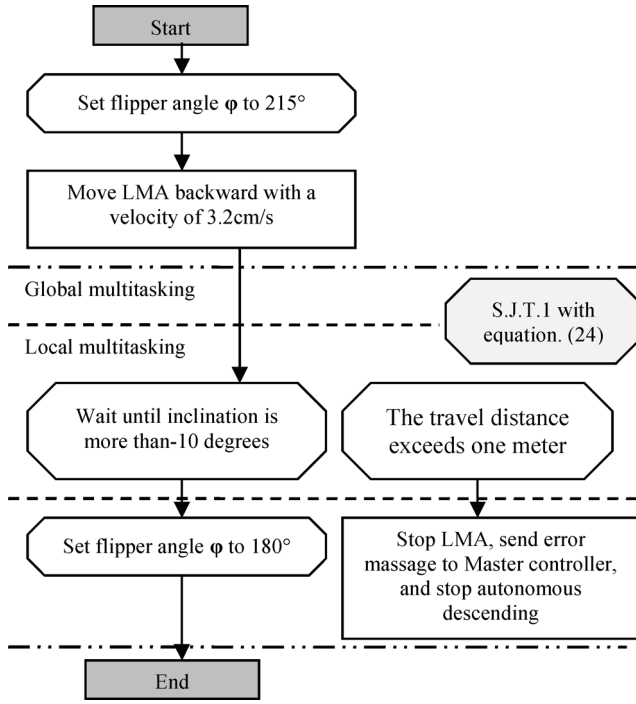


Fig. 20. Flowchart of riding on nose line of descending.

flipper tip touches the ground. The LMA stops autonomously, thus no interruption by the operator is required. In this stage, the stability judgment shown in Fig. 11(b) without Eq. (13) is used.

**4.2.3. Descending task stage 3: landing.** The landing procedure is accomplished by a backward sequence of the robot configurations in the riding on nose line stage of autonomous climbing as shown in Fig. 14. After the flipper touches the ground, it is rotated until its angle is set to  $160^\circ$  as shown in Fig. 14(b), and the LMA moves backwards until the inclination becomes less than  $\theta_1 + 5^\circ$ . A  $5^\circ$  margin is added to consider the settling time of the three-axis compass, and  $\theta_1$  is the recorded LMA inclination measured during the riding on nose line stage of autonomous climbing of stairs. During the motion, the stability judgment depicted in Fig. 11(a) with Eq. (24) is running.

Along with the stability judgment of Fig. 11(a) and Eq. (23), the flipper is rotated to set its angle to  $30^\circ$  (Fig. 14(a)) and the LMA moves 30 cm backwards or until its inclination is less than  $5^\circ$  in order to fully detach the robot from the stairs. Finally, the flipper is extended to the rear, and autonomous descending of stairs is completed.

## 5. Experimental Setup and Results

Experiments were performed in order to effectively implement and validate the stages required for autonomous climbing and descending of stairs. This involves step height measurement and up-to-date and accurate measurement of the robot's inclination in order to continuously evaluate the stability judgment equations derived in Section 3. In order to validate the effectiveness of the stability judgments, the filtered inclination signal is required to ensure that accurate robot inclination measurement is used. Therefore,

after the signal emanating from the inclinometer sensor is analyzed in Subsection 5.2, the stability judgments were validated in Subsection 5.3 in order to prove the successful implementation of autonomous climbing and descending of stairs. Several solutions to the problems that occurred during the implementation stage are also discussed.

### 5.1. Measurement of step height

The step height is measured every time autonomous climbing of stairs is activated, and used in the stability judgments equations. In this section, the method and equations to estimate the step height of the stairs are developed.

**5.1.1. Methodology.** As discussed in Subsection 4.1.1, after an initialization of autonomous climbing of stairs, the LMA moves backwards 10 cm from the first riser and its flipper rotates until it touches the first step edge. The flipper rotation torque is small enough such that the flipper stops rotating when it touches the step edge as shown in Fig. 12(b). In this configuration, the step height  $h$  is a function of the flipper angle  $\varphi$ . It is difficult to estimate the function mathematically since the elasticity of the tracks should be considered. Therefore, the function relating the step height  $h$  and the flipper angle  $\varphi$  was empirically estimated according to the experiment described below.

After several trials, in order to examine the relationship between step height and flipper angle, we observed that the relationship can be assumed as a linear function. In order to estimate the linear function, the least square method was used. The experiment to collect the data was done by changing the step height three times. For each step height, the algorithm from the measurement stage in autonomous climbing of stairs was followed, and the flipper angle was recorded when the flipper touched the step edge. This procedure was repeated five times for each step height, and the average of the five measured values was calculated, and the results tabulated in Table III. In the table, the recorded angles are  $\gamma = 180^\circ - \varphi$  with the average values rounded.

**5.1.2. Equation estimation.** The relationship between the step height  $h$  and flipper angle  $\varphi$  was assumed to be linear:

$$h = \alpha\gamma + \beta, \quad (26)$$

where  $\gamma = 180 - \varphi$ . With the least square method, the above parameters  $\alpha$  and  $\beta$  were estimated:

$$\alpha = \frac{\sum_{i=1}^n h_i \sum_{i=1}^n \gamma_i^2 - \sum_{i=1}^n \gamma_i \sum_{i=1}^n h_i \gamma_i}{n \sum_{i=1}^n \gamma_i^2 - \left( \sum_{i=1}^n \gamma_i \right)^2},$$

$$\beta = \frac{n \sum_{i=1}^n h_i \gamma_i - \sum_{i=1}^n h_i \sum_{i=1}^n \gamma_i}{n \sum_{i=1}^n \gamma_i^2 - \left( \sum_{i=1}^n \gamma_i \right)^2} \quad (27)$$

where  $n$  is the number of the data set. By substituting the data from Table III into Eq. (27), the parameters  $\alpha$  and  $\beta$  were found to be  $-0.563$  and  $105.8$ , respectively. Therefore, the

Table III. Angles  $\gamma$  (i.e.,  $180-\phi$ ) of step height experiments.

Data set $i$	Step height $h_i$ [cm]	Average $\gamma_i$ [degrees]
1	12.5	156
2	14.5	162
3	18.0	166

relationship of the flipper angle  $\phi$  and step height  $h$  is given by:

$$h = -0.563(180 - \phi) + 105.8 \quad (28)$$

**5.1.3. Accuracy.** The estimated step heights have an error of 1 cm at the most due to the treads on the tracks of the LMA. When the flipper engages the first step edge to measure the step height, if the treads are sandwiched between the tracks and the stair edge, the estimated value would be larger than the real height. Errors resulting from step height estimations were managed by adding margins to the range of the robot's COG. In the implementation of the stability judgments discussed in Subsection 5.3, it is shown that the LMA is successfully stopped on time to avoid flipping over even though the estimated step height has a 1 cm error.

## 5.2. Signal analysis and filters

Autonomous climbing strongly relies on the pitch, or inclination data from the three-axis compass embedded in the LMA chassis. The signal emanating from the compass was too noisy to be able to use it while the robot was moving on nose lines. Therefore, the signal was analyzed and algorithms and filters were designed in order to remove the noise effects.

**5.2.1. Signal analysis.** Figure 21(a) shows raw inclinations from the three-axis compass while the LMA was moving on the nose line as shown in Fig. 21(b). When the LMA is on the nose line, the inclination is supposed to provide readings indicating the slope of the nose line (i.e.,  $45^\circ$ ). However, it is observed that the signal is strongly disturbed by noise. During observations of the LMA in motion, three main factors were found to cause the fluctuations in the signal emanating from

the compass. Each factor and the mechanism causing it are explained below.

### (1) Slips between the treads and step edges

The pulses in Fig. 21(a) occur due to slip between the treads and the step edges. After each slipping event, the LMA re-engages the stairs with subsequent treads hooking onto the step edges. Slipping and re-engaging occur in a very short duration, forcing sudden accelerations to the LMA, which are picked up by the accelerometer in the 3-axis compass. As a result, the compass returns a strong pulse regarded as an inclination change, even though the overall inclination never changes.

### (2) Oscillation of the chassis

Approximately 4–7 Hz noise is created by the oscillation of the LMA's frame while it is moving on the nose line. At that time, the LMA is usually sustained by two-step edges as shown in Fig. 21(b) and oscillated about the pitch axis. The energy that causes oscillations to the LMA is produced by disengagements occurring between the step edges and some of the treads. When a tread is released from a step edge around the tip of the flipper, the tread slightly pushes the flipper up, which results in slight oscillations in the LMA chassis.

### (3) Position of the LMA on nose line

As shown in Fig. 22(a), the tracks between the flipper wheels and the rear wheels locally bend when a stair edge touches the tracks in that area. On the other hand, the tracks between the front and rear wheels are straightened by the bottom part of the LMA frame. Therefore, the compass shows a slightly larger value than the actual slope of the nose line. In cases when the step edges are positioned under the wheels as shown in Fig. 22(b), the inclination measured by the compass coincides with the actual slope of the nose line. In the figure, the magnitude of the local bending of the track is exaggerated for clarity.

The deviations in the inclinations caused by the LMA positions on the nose line can be measured by a simple experiment, in which the LMA moves forward 1 cm, stops for 5 s, records the inclination data and repeats. By stopping

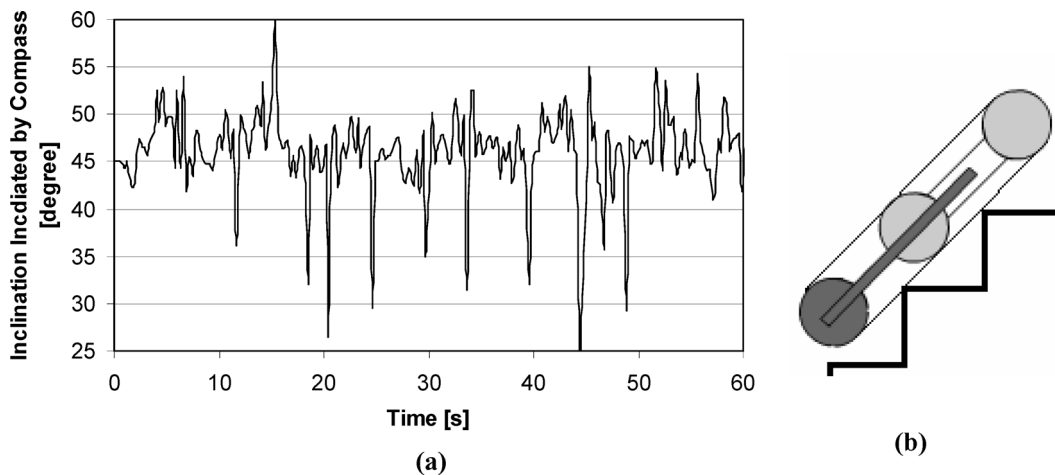


Fig. 21. (a) Raw data from compass; (b) LMA on nose line.

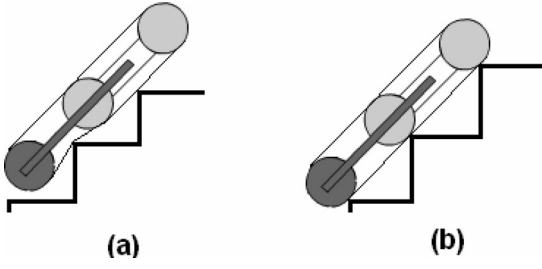


Fig. 22. Inclination changes with the position of the LMA.

for 5 s before the measurements are recorded, the noise caused by the tracks' slips and chassis oscillations can be removed. We observed that the deviations from the nose line slope are within  $1.5^\circ$  according to the recorded inclinations shown in Fig. 23. We also observed that the measured signal has a wave period. The frequency of the signal is calculated from the local minimums listed in Table IV. The wavelengths are measured as the distance traveled between two adjacent local minimums. Their average is 25.5 cm, and it is found to be the same as the distance between two adjacent step edges (25.5 cm). The mechanism causing the inclination changes created by the LMA positions on the nose line can be effectively validated. Using the following equation, the fundamental frequency of the waves caused by the factor "position of LMA on Nose Line" is calculated:

$$f = \frac{v(n-1)}{\sum_{i=2}^n (d_i - d_{i-1})} = 0.128 \text{ Hz}, \quad (29)$$

where  $v$  is the velocity of the LMA,  $n$  is the total number of local minimums, and  $d_i$  is the distances traveled as defined in Table IV.

Since the wavelengths and the distance between adjacent step edges are the same, the following equation is equivalent to Eq. (29):

$$f = \frac{v}{d_{edge}}, \quad (30)$$

where  $d_{edge}$  is the distance between two adjacent step edges. Therefore, the corresponding fundamental frequency is predictable from the dimension of the stairs. From the condition of Eq. (12), the longest step edge distance the

Table IV. Local minimums and wavelengths.

Data number $i$	Local minimum $\theta_{\min}$ [degree]	Travel distance $d_i$ [cm]	Wavelength $d_i - d_{i-1}$ [cm]
1	44.1	18	
2	44.2	44	26
3	44.4	69	25

LMA can climb is 29.6 [cm]. By substituting this value and the robot's velocity 3.2 [cm/s] into Eq. (30), we obtain the minimal fundamental frequency  $f_{\min} = v/d_{edge,\max} = 0.108 \text{ Hz}$  due to inclination changes caused by the factor "LMA position on a nose line". Similarly, the maximum fundamental frequency  $f_{\max} = v/d_{edge,\min} = 0.137 \text{ Hz}$  is obtained from the shortest step edges (23.3 cm), which is calculated from the stair dimensions constraints.

The calculated fundamental frequency in Eq. (29) is viewed by spectrum analysis, using Burg's algorithm.<sup>17</sup> The algorithm is a parametric spectral estimation method, by which an autoregressive (AR) linear prediction filter model is used to model an input signal for estimating the power spectral density (PSD).<sup>17</sup> Before the spectrum analysis is performed, the DC value in the signal of Fig. 21(a) was removed by subtracting its average inclination ( $46.1^\circ$ ). Figure 24 shows the spectrum analysis. The order of the AR model of the Burg algorithm used was 30 and the Fast Fourier Transform (FFT) length was 1024. The sampling frequency of the inclination was 4 Hz. The strongest PSD is seen around 0.13 Hz, which is almost the same as the value calculated with Eq. (29)—namely, 0.128 Hz.

**5.2.2. Noise elimination.** This section shows the design of two serially connected filters in order to remove the noise from the measured inclination signal to guarantee stable autonomous climbing.

### (1) Filter 1: algorithm for pulse elimination

With this filter, the abrupt pulses created by slip occurring between the treads and the step edges were removed. In this algorithm, if the difference between new inclination data from the compass and the previous value is  $5^\circ$  or more, the output of Filter 1 holds the same value; otherwise, the new value is outputted. This means that the data points from

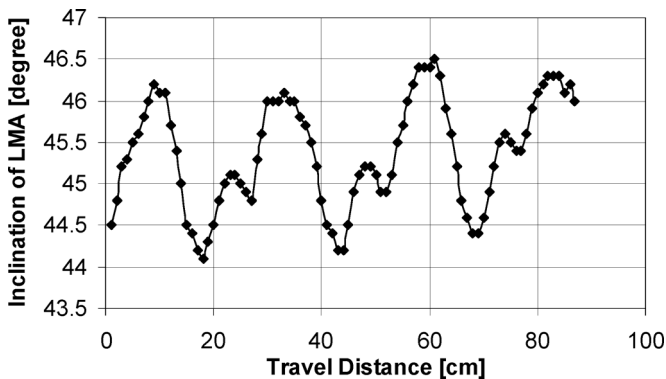


Fig. 23. Effect of LMA position on nose line.

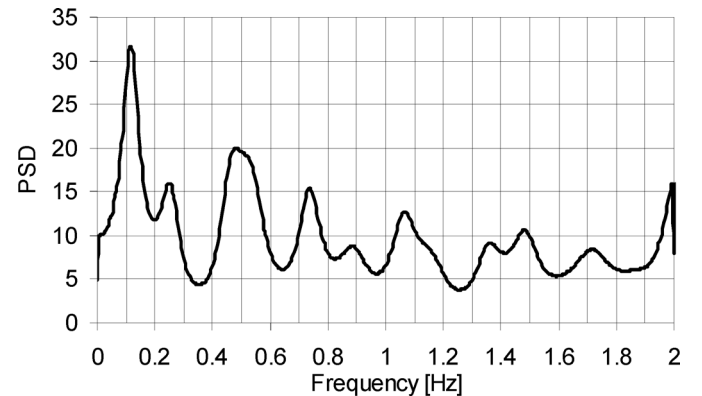


Fig. 24. Spectrum analysis of raw data from the compass.

the compass are blocked until they settle within a certain range, thereby eliminating pulses having a magnitude of  $5^\circ$  or greater. The flowchart describing the implementation of this algorithm is shown in Fig. 25. Figure 26 shows the simulated output of Filter 1 with its input being the raw data from the compass as shown in Fig. 21(a). It can be seen that the pulses are being effectively truncated.

## (2) Filter 2: digital filter

The second filter is a low-pass digital filter used to remove the noise caused by the oscillation of the chassis and other miscellaneous factors such as effects caused by electronic devices. The deviations created by the LMA position on a nose line are not considered noise, but rather real inclination changes that might cause it to flip over in some cases. Therefore, Filter 2 should pass those deviations. By considering their highest frequency (0.137 Hz) as calculated with Eq. (30), the filter's cut off frequency ( $f_c$ ) was set to 0.20 Hz.

The digital filter is a finite impulse response (FIR) filter using a Gaussian window for its design. The order of the filter coefficients was set to four, based on a trade off between the filter quality and a time delay caused by the filter. If the order was larger, the transition area between the pass band and the stop band would be narrower in the frequency response of the filter. However, it would cause a larger time delay, which was not suitable for the LMA especially due to the requirement that it needs to stop in an emergency situation such as to prevent falling or tipping over.

The signal processed by the designed filter is expressed by the following equation:

$$\hat{\theta}_n = \sum_{i=0}^4 \theta_{n-i} b_i, \quad (31)$$

where  $\hat{\theta}$  is the output of Filter 2 (or processed signal),  $\theta$  is the output of Filter 1 (or input of filter 2),  $b$  is a filter coefficient and  $n$  expresses the  $n^{\text{th}}$  data point. The filter coefficients were calculated and found to be:  $b_0 = b_4 = 0.1627$ ,  $b_1 = b_3 = 0.2175$ , and  $b_2 = 0.2395$ . The frequency response of this filter confirmed that the filter is a LPF.

The two filters designed above (i.e., Filter 1 and Filter 2) are connected in series resulting in high frequency components being cut off after impulses are eliminated. With this set of filters, the raw data shown in Fig. 21(a) become the signal shown in Fig. 27. The output deviations from the slope of the nose line are restricted within  $7^\circ$ .

**5.2.3. Effectiveness of noise elimination.** In order to validate the effectiveness of Filters 1 and 2, new raw robot inclination signal and its filtered signal were directly read from the LMA sensors. The signals from the LMA shown in Fig. 28 demonstrate the successful removal of the pulses around 66.5, 70.5, 79.5, 88, 90.5 and 95 [s].

## 5.3. Validation of stability judgment

With the filtered robot inclination signal, as discussed in the previous subsection, the stability judgment equations derived

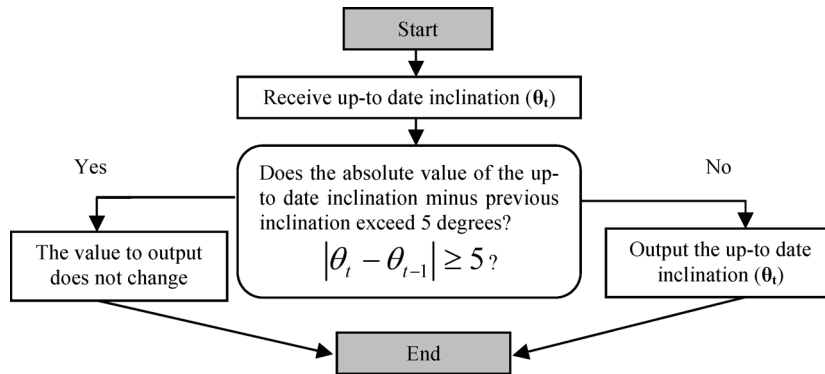


Fig. 25. Algorithm of filter 1.

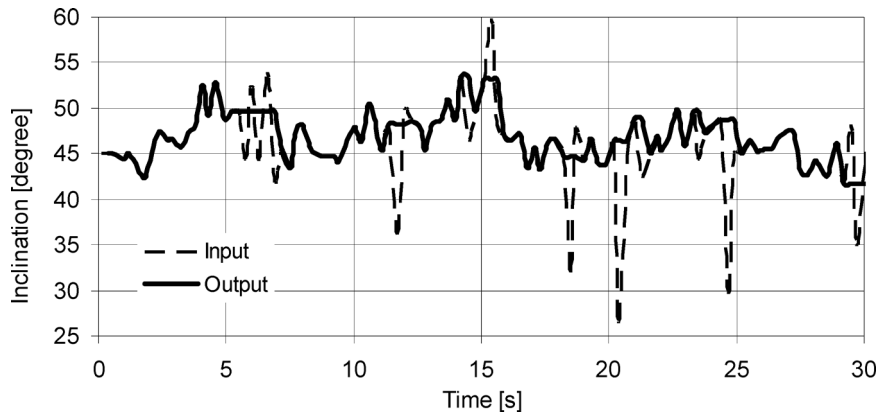


Fig. 26. Effects of Filter 1.

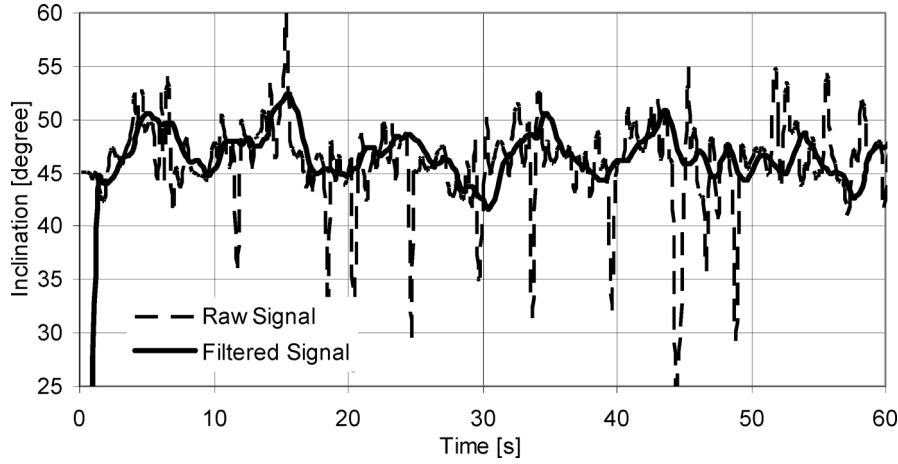


Fig. 27. Combined effect of Filters 1 and 2 connected in series.

in Section 3 are analyzed. In the analysis, we considered a COG range with margins for  $G_{y,max}$  and  $G_{x,min}$  to be 6.5 cm and 1.3 cm, respectively. The suitability of the margins is also discussed.

**5.3.1. Stability judgment equation of LMA with flipper suspended above the platform.** The stabilizing condition derived in Eq. (23) applies to the case when the rear wheels of the LMA are on the ground with its flipper suspended in the air. Rearranging Eq. (23) and solving for  $\theta$  yields:

$$\theta < \tan^{-1}(G_{x,min}/G_{y,max}). \quad (32)$$

With the COG range data outlined in Table II, the value  $\theta_1 < 85.5^\circ$  satisfies the above condition. If margins (6.5 cm for  $G_{y,max}$  and 1.3 cm for  $G_{x,min}$ ) are added such that the two parameters  $G_{y,max}$  and  $G_{x,min}$  become 8.0 cm and 18.0 cm, respectively, the condition  $\theta_2 < 66^\circ$  for the stability of the LMA is obtained. This threshold cannot be implemented in the stability judgments since the three-axis compass working inclination range is between  $-60$  and  $60^\circ$ . Therefore, the condition  $\theta_3 < 59.5^\circ$  has been used instead. The difference between the two thresholds  $\theta_1$  and  $\theta_3$  (i.e.,  $26^\circ$ ) is utilized as a margin in order to stop the LMA before it flips over.

**5.3.2. Stability judgment equation of LMA with flipper at the rear.** The stabilizing condition derived in Eq. (24) applies to the case when the flipper is positioned at the rear in order to support the robot's platform.

$$G_{x,min} > G_{y,max} \tan \theta + \frac{L}{2} + l(\varphi) \frac{\cos(\theta + \varphi)}{\cos \theta} \quad (24)$$

Equation (24) is plotted and visualized in Fig. 29 with the vertical axis showing inclinations of the robot and the horizontal axis representing flipper angles. The three lines in the graph represent the thresholds of the LMA's stability to satisfy Eq. (24) under each condition. The blue line represents the case where the range of the COG has no margins. The red line represents the case when margins are incorporated in the COG range, and the black line represents the case where the signal range of the compass ( $-60$  to  $60^\circ$ ) is considered. In the implemented stability judgments, if the compass indicates an inclination larger than the threshold of the black line, the LMA is stopped. Therefore, the white area represents the implemented stable region, and the gray area shows the unstable region under which the LMA would flip over. The other regions are margins. The yellow margin results from the restriction of the compass range, and the sky blue area is the result of the margins of the COG range.

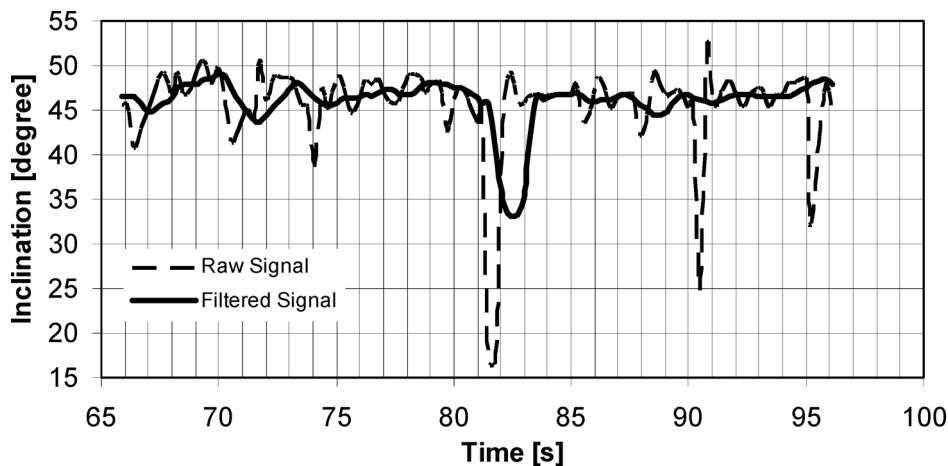


Fig. 28. Validation of noise elimination.

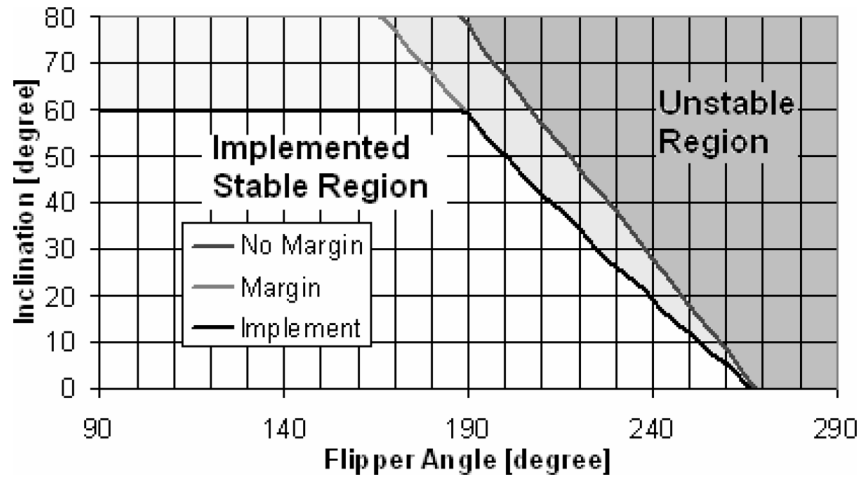


Fig. 29. Thresholds of stability judgment for LMA with flipper on ground.

While the stability judgments are running, the flipper angle is not exceeding  $225^\circ$ . This means that the judgment always has at least  $10^\circ$  margin to stop the LMA before it flips over.

5.3.3. *Stability judgment equations of LMA on nose line.*  
 Stability judgment Eqs.(13) and (25) apply to the case when the LMA is going up or down on a nose line.

$$\theta \geq \sin^{-1} \frac{2h}{L/2 + l(180^\circ) - r}. \quad (13)$$

$$G_{x \min} > \frac{L}{2} - l(180^\circ) + \frac{h}{\sin \theta} + (G_{y \max} + r) \tan \theta \quad (25)$$

Equations (13) and (25) are plotted and visualized in Fig. 30 with the vertical axis representing the inclinations of the robot and the horizontal axis representing the step height. Equation (25) defines the upper limit of inclinations, to ensure that the LMA is stable on nose lines. When the margins of the COG range are considered, the threshold to flip over is represented by the red line in the Fig. 30; otherwise the threshold is represented by the blue line. Therefore, the

region between the blue and red lines is the resultant margin in the inclination domain. The black line is the threshold implemented in the stability judgments by considering the range of the three-axis compass ( $-60^\circ$  to  $60^\circ$ ). The yellow region is the margin produced by the compass restriction. The two margin regions create at least  $13^\circ$  margin in the inclination domain within the expected estimated step heights (i.e., 11 cm to 19 cm). With these large margins, the LMA can be successfully stopped before flipping over even with the 1 cm error in the step height estimation, as discussed in Subsection 5.1. For example, the difference of thresholds without margins at step heights of 17 cm and 18 cm is only  $1^\circ$  in terms of inclinations. This means that there is still a  $12^\circ$  margin, even if the LMA detects a 17 cm step height as 18 cm step height.

Equation (13) is represented by the black dashed line in Fig. 30. This line indicates the minimum inclinations in order to remain stable. The area beneath the dashed line is an unstable region. Furthermore, the condition of Eq. (13) is a moderate constraint and already includes some margins. Thus, no additional margins were added to the bottom limit in Fig. 30.

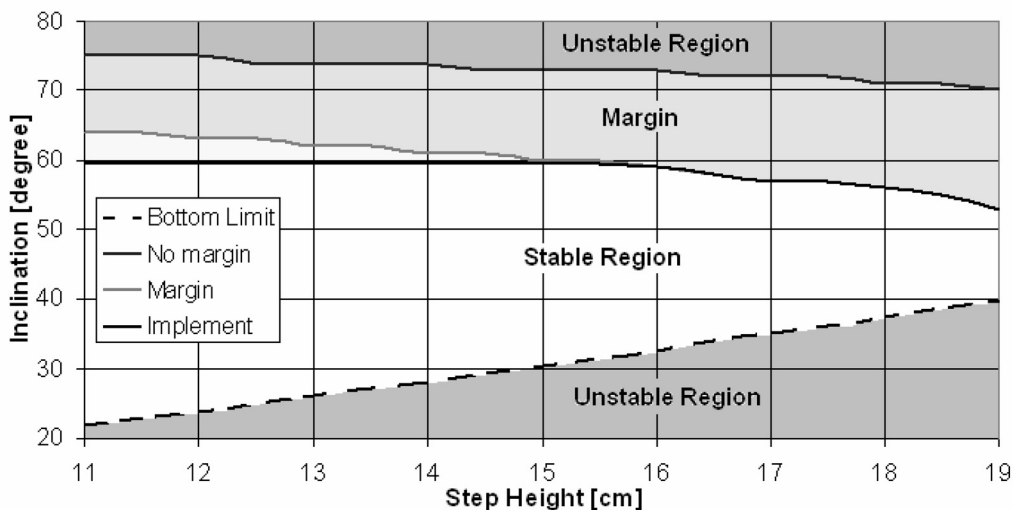


Fig. 30. Thresholds of stability judgment of the LMA on nose line.

**5.3.4. Effectiveness of stability judgment.** The effectiveness of the stability judgments to stop the LMA before it flips over was examined through experiments. First, the LMA was set such that the front wheels are engaged on the obstacle and the rear wheels were on the ground as shown in Fig. 31(a), (b) or (c), depending on the stability judgment equation to be examined (i.e., Eqs. (23), (24) or (25), respectively). Each flipper angle in Fig. 31(a), (b), and (c) was 45, 160 and 180°, respectively. In each case, the LMA moved forward, thereby activating the corresponding judgment equation.

According to the experiments performed for stability judgment with Eqs. (23) and (24), it was confirmed that the LMA was successfully stopped without any flip-over events. In the case of Eq. (25) as well, the LMA halted its motion without flipping-over. The filtered inclination signal during the test is shown in Fig. 32. The LMA was stopped at 1.6 s when the filtered inclination measurement exceeded 56°. The 56° threshold can be calculated by substituting a step height of 18 cm into Eq. (25) (or by referring to Fig. 30). The real inclination of the LMA after the stop was 59.9°. The 4° difference between the threshold and the inclination at the stopping time resulted from the settling time of the compass (1750 ms), but this difference was allowable since the stability judgment equation had a 13° margin.

#### 5.4. Programming

The programs for the autonomous mode, by which autonomous climbing and descending are executed, are introduced in this section. When the LMA is turned on, the manual mode, with which the operator operates the LMA with the use of the remote controller, is activated. When the operator selects the autonomous mode on the

remote controller, a frame with the commands to activate the autonomous mode is transmitted to the slave controller.

Once the autonomous mode is activated, the slave controller idles and waits for a frame by which the LMA starts to climb or descend stairs autonomously. The frame has information on the direction (i.e., climbing or descending), obstacle type (i.e., stairs or cant), procedure stage, and status (i.e., idling or running). While the LMA is moving autonomously, there are five tasks the computer performs simultaneously: (i) run algorithms to follow autonomous climbing or descending; (ii) incorporate the stability judgment equations in the algorithms; (iii) send requests to the sensor processor (every 100 ms); (iv) receive data from the remote controller or the sensor processor; (v) perform calculations in order to filter the inclination signal from the compass (every 250 ms).

Receiving data from the remote controller is required in order to stop the LMA in cases of emergency. The data coming from the sensor processor is the robot's inclinations.

When autonomous climbing and descending are completed or interrupted by stability judgments, a frame is sent to the remote controller to idle the LMA and wait for a command from the operator. During the idling of the autonomous mode, the operator can shift to the manual mode with the remote controller.

## 6. Conclusions

In this paper, a method of autonomous climbing and descending of stairs was introduced. Stability judgment equations were formulated and used as conditions to prevent tip-over and ensure stability of the mobile robot. The effectiveness of these equations was determined by adding margins to the range of variation of the mobile robot's center of gravity (COG). In order to execute the procedures for climbing and descending of stairs, methods of measuring the step height of the stairs and calculating the mobile robot's COG were introduced. Furthermore, the noisy signal emanating from the inclinometer sensor was analyzed, and solutions to remove it with designed filters and algorithms were suggested and implemented in order to ensure accurate robot inclination measurement. With the measurements of the step height, robot's COG, and filtered robot inclination signal, the stability judgments were implemented on the LMA for autonomous climbing and descending of stairs. In order to examine the effectiveness of the entire procedure, the LMA was tested, and the results analyzed. In all cases, it was observed that autonomous climbing and descending was successfully completed. Moreover, the LMA stopped automatically when it perceived danger of falling or tipping over. The implementation of the autonomous climbing and descending of stairs greatly increases the controllability of the procedure and greatly decreases the operator's burden.

## Acknowledgments

This work was partially supported by Natural Sciences and Engineering Research Council of Canada (NSERC)—grant # 480553, and Engineering Services Inc. (ESI).

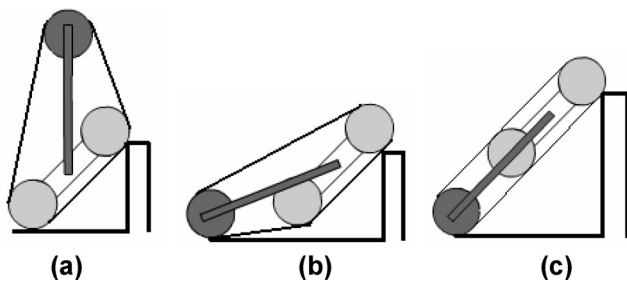


Fig. 31. Initial configurations for stability judgment evaluations.

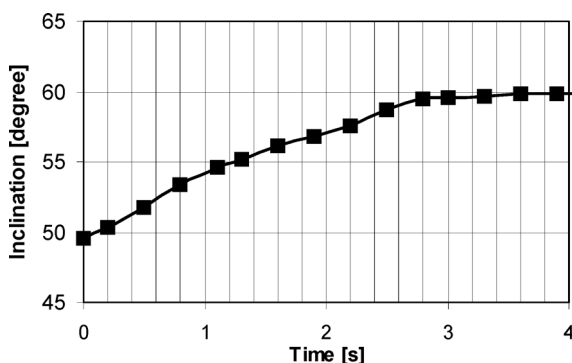


Fig. 32. Inclinations during the test of stability judgment with Eq. (25).

## References

1. A. A. Goldenberg and J. Lin, "Variable Configuration Articulated Tracked Vehicle," US Patent Application # 11/196,486, August 4, 2005. Engineering Services Inc. <http://www.esit.com>
2. J. Liu, Y. Wang, S. Ma and B. Li, "Analysis of Stair-Climbing Ability for a Tracked Reconfigurable Modular Robot," *Proceedings of the 2005 IEEE Int. Workshop on Safety and Rescue Robotics*, Kobe, Japan (2005) pp. 36–41.
3. J. Gaston, K. Raahemifar and P. Hiscocks, "A cooperative network of reconfigurable stair-climbing robots," *IEEE Int. Symp on Circuits and Systems* (2006) pp. 2553–2556.
4. S. A. Stoeter and N. Papanikolopoulos, "Autonomous stair-climbing with miniature jumping robots," *IEEE Trans. Syst. Man Cybern.—Part B: Cybern.* **35**(2), 313–325 (2005).
5. X. Duan, Q. Huang, N. Rahman, J. Li and Jingtao Li, "MOBIT, A small Wheel–Track–Leg Mobile Robot," *Proceedings of the 6th Congress on Intelligent Control and Automation*, Kos Greece (2006) pp. 9159–9163.
6. D. G. Gweon and H. D. Kim, "Development of a mobile robot controlled by three motors for a hostile environment," *Mechatronics* **2**(1), 43–64 (1992).
7. W. Lee, S. Kang, M. Kim and K. Shin, "Rough Terrain Negotiable Mobile Platform with Passively Adaptive Double-Tracks and its Application to Rescue Missions," *International Conference on Robotics and Automation*, Barcelona, Spain. (2005) pp. 1591–1596.
8. B. Yamauchi, "PackBot: A Versatile Platform for Military Robotics," *Proceedings of SPIE–Unmanned Ground Vehicle Technology VI*, Orlando, FL (2004) pp. 228–237.
9. T. Frost, C. Norman, S. Pratt and B. Yamauchi, "Derived Performance Metrics and Measurements Compared to Field Experience for the PackBot," *Proceedings of the 2002 PerMIS Workshop*, Gaithersburg, MD, USA (2002) pp. 201–208.
10. Y. Xiong and L. Matthies, "Vision-Guided Autonomous Stair Climbing," *International Conference on Robotics and Automation*, San Francisco, CA, USA (2000) pp. 1842–1847.
11. J. D. Martens and W. S. Newman, "Stabilization of a Mobile Robot Climbing Stairs," *IEEE International Conference on Robotics and Automation*, San Diego, CA, USA. (1994) pp. 2501–2507.
12. Logosol Homepage, Logosol Inc., <http://www.logosolinc.com>, October 2007.
13. J. Lin, "Studies on Movement Conditions of Tracked Vehicles with Variable Configuration," Engineering Services Inc., October 2004, internal report.
14. J. Lin, "Supplement 1—on "Movement Conditions of Tracked Vehicles," Engineering Serviced Inc., October 20, 2004, internal report.
15. J. Lin, "Determining the Technology Parameters of LMA-2 Vehicle Based on Static Mechanics Analysis," Eng. Services Inc., May 2004, internal report.
16. J. R. Davis, "Center of Gravity: How to calculate where it is," <http://www.msgroup.org/TIP106.html>, October 2007.
17. MATLAB Signal Processing Toolbox, User's Guide Version 5, MATLAB Help for "pburg" function (Burg Method), The MathWorks.